Helge Ræder,[1,2,3] Fiona E. McAllister,[4] Erling Tjora,[2,3] Shweta Bhatt,[1] Ingfrid Haldorsen,[5,6] Jiang Hu,[1] Stefan M. Willems,[4] Mette Vesterhus,[7] Abdelfattah El Ouaamari,[1] Manway Liu,[8] Maria B. Ræder,[3] Heike Immervoll,[9,10,11] Dag Hoem,[12] Georg Dimcevski,[7] Pål R. Njølstad,[2,3] Anders Molven,[9,10] Steven P. Gygi,[4] and Rohit N. Kulkarni[1]

# Carboxyl-Ester Lipase Maturity-Onset Diabetes of the Young Is Associated With Development of Pancreatic Cysts and Upregulated MAPK Signaling in Secretin-Stimulated Duodenal Fluid

**Carboxyl-ester lipase (CEL) maturity-onset diabetes of the young (MODY) is a monogenic form of diabetes and pancreatic exocrine dysfunction due to mutations in the *CEL* gene encoding CEL. The pathogenic mechanism for diabetes development is unknown. Since *CEL* is expressed mainly in pancreatic acinar cells, we asked whether we could find structural pancreatic changes in CEL-MODY subjects during the course of diabetes development. Furthermore, we hypothesized that the diseased pancreas releases proteins that are detectable in pancreatic fluid and potentially reflect activation or inactivation of disease-specific pathways. We therefore investigated nondiabetic and diabetic *CEL*-mutation carriers by pancreatic imaging studies and secretin-stimulated duodenal juice sampling. The secretin-stimulated duodenal juice was studied using cytokine assays, mass spectrometry (MS) proteomics, and multiplexed MS-based measurement of kinase activities. We identified multiple pancreatic cysts in all eight diabetic mutation carriers but not in any of the four nondiabetic mutation carriers or the six healthy controls. Furthermore, we identified upregulated mitogen-activated protein kinase (MAPK) target proteins and MAPK-driven cytokines and increased MAPK activity in the secretin-stimulated duodenal juice. These findings show that subjects with**

[1]Section of Islet Cell Biology and Regenerative Medicine, Joslin Diabetes Center, Harvard Medical School, Boston, MA
[2]Department of Pediatrics, Haukeland University Hospital, Bergen, Norway
[3]KG Jebsen Center for Diabetes Research, Department of Clinical Science, University of Bergen, Bergen, Norway
[4]Department of Cell Biology, Harvard Medical School, Boston, MA
[5]Department of Radiology, Haukeland University Hospital, Bergen, Norway
[6]Section for Radiology, Department of Clinical Medicine, University of Bergen, Bergen, Norway
[7]Department of Medicine, Haukeland University Hospital, Bergen, Norway
[8]Department of Biomedical Engineering, Boston University, Boston, MA
[9]Gade Laboratory for Pathology, Department of Clinical Medicine, University of Bergen, Bergen, Norway
[10]Department of Pathology, Haukeland University Hospital, Bergen, Norway
[11]Department of Pathology, Ålesund Hospital, Ålesund, Norway
[12]Department of Surgery, Haukeland University Hospital, Bergen, Norway

Corresponding author: Helge Ræder, helge.rader@uib.no.

Received 28 June 2013 and accepted 16 September 2013.

This article contains Supplementary Data online at http://diabetes.diabetesjournals.org/lookup/suppl/doi:10.2337/db13-1012/-/DC1.

F.E.M. and E.T. contributed equally.

**CEL-MODY develop multiple pancreatic cysts by the time they develop diabetes and that upregulated MAPK signaling in the pancreatic secretome may reflect the pathophysiological development of pancreatic cysts and diabetes.**

*Diabetes 2014;63:259–269 | DOI: 10.2337/db13-1012*

Studies of patients with maturity-onset diabetes of the young (MODY) have provided important insight into disease mechanisms of pancreatic β-cell failure and diabetes development and also contributed to novel treatment strategies based on this insight (1,2). We have previously reported two families with a human monogenic syndrome of diabetes and pancreatic exocrine dysfunction (MODY type 8, MODY8; carboxyl-ester lipase [CEL]-MODY; OMIM 609812) caused by mutations in the CEL gene, *CEL* (3). Patients with *CEL* mutations develop pancreatic exocrine dysfunction in early childhood (as measured by low fecal elastase levels), accumulate pancreatic fatty tissue, and develop diabetes and clinical malabsorption in their fourth decade of life (3,4). The gene encoding *CEL* is primarily expressed in pancreatic acinar cells and lactating mammary tissue and encodes a digestive enzyme with a role in cholesterol ester digestion (5). Studies of animal models have not been able to explain the disease mechanism of diabetes development in CEL-MODY (6,7), but cellular studies indicate that mutated CEL protein is misfolded (8). Hence, to gain further insight into the disease mechanism, we further studied human *CEL*-mutation carriers using radiological methods and secretin-stimulated duodenal juice to examine the pancreatic proteome (9). We hypothesized that the diseased pancreas releases proteins that are detectable in pancreatic fluid and potentially reflect activation or inactivation of disease-specific pathways. To optimize the accuracy of the proteomics studies, we applied triple-stage mass spectrometry (MS) (10) and complemented this approach with cytokine assays and MS-based multiplex kinase activity assays (11) to cross-validate our findings.

## RESEARCH DESIGN AND METHODS

### Patients

We have previously reported various clinical characteristics for the *CEL*-mutation-carrying subjects (3). In this study, the studied *CEL*-mutation-carrying subjects (*CEL*+) were denoted with the prefix *D* if they had manifest diabetes (D1, D2, D3, or D4), with the prefix *P* if they had not yet developed diabetes (P1 or P2), or with the prefix *C* for the patient with pancreatic ductal adenocarcinoma (C1). The Supplementary Data contain the corresponding pedigree information. The nonfamily controls were denoted with the prefix *N* (N1, N2, N3, or N4) for controls in the duodenal juice studies. We sampled duodenal juice from the patients by endoscopy. To enrich for pancreatic factors, we administered intravenous secretin (Secrelux, Sanofi, Germany; 1 cU/kg, maximum 70 cU) to the patients and sampled duodenal juice 30 to 45 min later since it has been shown that there is a peak secretion from pancreas in this time interval (12,13). The controls for the secretin-stimulated duodenal juice studies were recruited from volunteers. The single pancreatic juice specimen from a *CEL*-mutation carrier with pancreatic ductal adenocarcinoma was collected during a classical Whipple procedure. All studies were approved by the Norwegian Regional Committee for Research Ethics and the institutional review board at the Joslin Diabetes Center and performed according to the Helsinki Declaration. We obtained written informed consent from subjects or their parents. Patients were of Northern European descent and recruited from the Norwegian MODY Registry.

### Protocol for Pancreatic Imaging

Magnetic resonance imaging was performed on a 1.5 T Siemens Avanto running Syngo Magnetic Resonance B17 (Erlagen, Germany) using a 12-channel body coil. For clinical and anatomical evaluation of the pancreas, a standard abdominal protocol was used: axial true fast imaging with steady-state precision (repetition time = 2.79 ms, echo time = 1.17 ms, slice thickness = 4.0 mm, spacing = 0, $\alpha = 63°$, field of view = 380 × 380 $mm^2$, matrix = 156 × 192, acquisition time = 15 s) and axial fat-saturated T2-weighted imaging (repetition time = 1,000 ms, echo time = 90 ms, slice thickness = 5 mm, spacing = 0, $\alpha = 150°$, field of view = 350 × 350 $mm^2$, matrix = 256 × 256, acquisition time = 24 s). For evaluation of the pancreatic and biliary ducts, magnetic resonance cholangiopancreatography was performed: coronal T2-weighted imaging (repetition time = 2,000 ms, echo time = 691 ms, slice thickness = 1.1 mm, spacing = 0, $\alpha = 140°$, field of view = 280 × 280 $mm^2$, matrix = 320 × 320, acquisition time = 5.23 min) with maximum intensity projection and multiplanar reformatting.

### Cytokine Assay

Forty-two cytokines were measured in secretin-stimulated duodenal juice samples (sample volume of 25 μL), using the MILLIPLEX MAP Human Cytokine/Chemokine-Premixed 42 Plex kit from Millipore (Billerica, MA). This 42-plex kit was used to measure the concentrations of epidermal growth factor, eotaxin, fibroblast growth factor-2, Flt-3 ligand, fractalkine, granulocyte colony–stimulating factor, granulocyte-macrophage colony–stimulating factor, growth-related oncogene (GRO), interferon-α2, interferon-γ, interleukin (IL)-10, IL-12 (p40), IL-12 (p70), IL-13, IL-15, IL-17, IL-1Rα, IL-1α, IL-1β, IL-2, IL-3, IL-4, IL-5, IL-6, IL-7, IL-8, IL-9, IP-10, monocyte chemoattractant protein (MCP)-1, MCP-3, macrophage-derived chemokine (CCL22), macrophage inflammatory protein-1α, macrophage inflammatory protein-1β, platelet-derived growth factor-AA, platelet-derived growth factor-AB/BB, regulated on activation

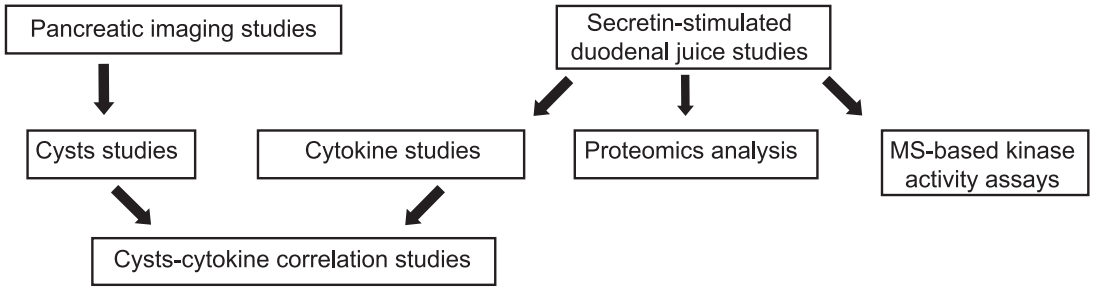


**Figure 1**—Overview of the multimodal systems biology approach. A systems biology approach using secretin-stimulated duodenal juice from subjects in a CEL-MODY family to discover early markers in pancreatic disease development by proteomics methods.

normal T cell expressed and secreted, transforming growth factor-α, tumor necrosis factor-α, tumor necrosis factor-β, vascular endothelial growth factor, soluble CD40 ligand, and soluble IL-2 receptor α. All samples were analyzed with a Luminex 200 xMAP system, and MILLIPLEX Analyst Software (VigeneTech, Carlisle, MA) was used to analyze the results.

### Proteolytic Degradation Assay

A set of 45 synthetic peptide substrates, each at 1 μmol/L, were incubated with 10 μg pancreatic fluid and reaction buffer containing Tris-Cl (25 mmol/L, pH 7.5), $MgCl_2$ (7.5 mmol/L), EGTA (0.2 mmol/L), β-glycerophosphate (7.5 mmol/L), $Na_3VO_4$ (0.1 mmol/L), and dithiothreitol (0.1 mmol/L). The reaction was incubated at room temperature for 0, 15, and 60 min, after which the reaction was quenched with 100 μL of 1% trifluoroacetic acid. Twenty-five picomoles of internal standard stable-isotope-labeled substrate peptides were spiked into the quenched reaction. The solution was desalted using Sep-Pak C18 50 mg cartridges (Waters, Milford, MA) and dried using vacuum

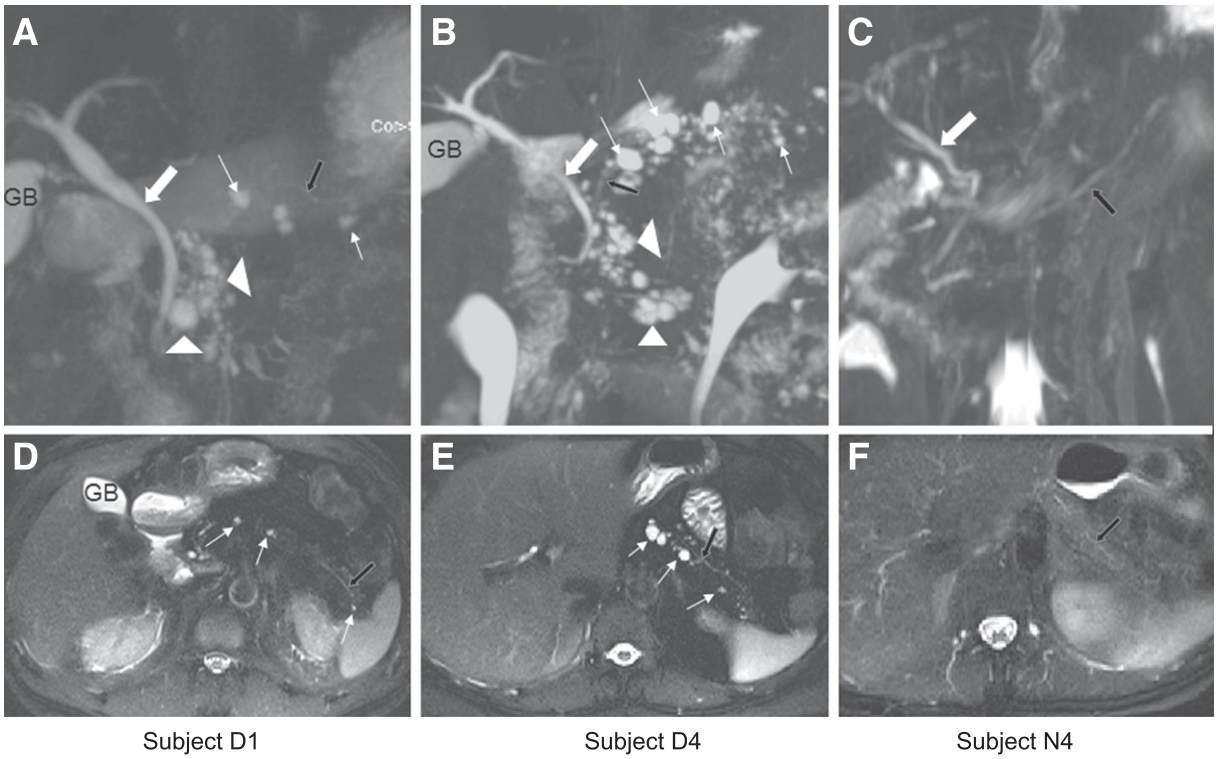


**Figure 2**—The magnetic resonance imaging of pancreatic cysts in *CEL*-mutation carriers. Magnetic resonance cholangiopancreatography (*A–C*) and axial fat-saturated T2-weighted imaging (*D–F*) at the level of the pancreatic body in two *CEL*-mutation carriers (*A* and *D*, *B* and *E*) and a normal control (*C* and *F*). Both mutation carriers had multiple cystic lesions within the pancreatic body and tail (white thin arrows, *A* and *B*, *D* and *E*) as well as in the pancreatic head (arrowheads, *A* and *B*). The pancreatic ducts (filled black arrows) and common bile ducts (filled white arrows) have normal caliper (*A* and *B*, *D* and *E*) similar to that in the control (*C* and *F*). The alphanumeric codes refer to the subject designation explained in RESEARCH DESIGN AND METHODS. GB, gallbladder.

centrifugation. The desalted sample was then resuspended in 100 μL of 5% formic acid, of which 2 μL was then subjected to analysis by MS. Technical duplicates were performed for each sample at each time point. The peptides from proteolytic degradation assays were analyzed by liquid chromatography (LC)-MS on a high-resolution Exactive Orbitrap mass spectrometer (Thermo Scientific, Rockford, IL). Briefly, a 45-min gradient was used to separate the peptides from 10–37% solvent B (0.125% formic acid in acetonitrile) at a flow rate of 300 mL/min. LC-MS data were collected from 350–1,500 mass-to-charge ratios, and the extracted ion chromatograms of the light and heavy peptides were used to quantitate the extent of peptide degradation, respectively. Data analysis was performed using Pinpoint (Thermo).

### Quantitative Proteomics of Pancreatic Juice Using Tandem Mass Tag Labeling

Pancreatic juice (100 μL) from six subjects was purified using methanol/chloroform precipitation. The purified protein pellets were each resuspended in 100 μL of 50 mmol/L HEPES, 4 mol/L urea, pH 8.5. The protein concentration was determined using Bradford protein assay (Pierce). The cysteine residues were reduced and alkylated with dithiothreitol (5 mmol/L) and iodoacetamide (15 mmol/L), respectively, prior to digestion with LysC (Wako, Japan) in a 1:100 LysC-to-protein ratio. Following digestion overnight, the digest was acidified with formic acid prior to desalting with C18 solid-phase extraction (Sep-Pak, Waters). The desalted peptides were then resuspended in 100 μL of 50 mmol/L HEPES, pH 8.5, and each sample was labeled with one of the six-plex tandem mass tag (TMT) reagents (Thermo) for 1 h at room temperature. The TMT-labeled peptides were purified and fractionated by strong cation exchange chromatography, and 14 fractions were analyzed by LC-MS/MS on an LTQ-Orbitrap Velos mass spectrometer. A triple-stage MS method developed recently by the laboratory was used to overcome the interference problem in acquisition of TMT data as described (10). Further experimental details for the proteomics and immunoblotting experiments, kinase activity assay (14), and proteolytic degradation assays are outlined in the Supplementary Appendix. Details for the database searches and filtering and quantification for the proteomics experiments are also outlined in the Supplementary Data, but briefly, two different types of searches (LysC

**Table 1—Clinical characteristics of *CEL*-mutation carriers and controls**

| Status | Sex | Age (years) | Fecal elastase (μg/g) | Diabetes | Diabetes duration (years) | Number of cysts | Largest cyst diameter (mm) | Pancreatic duct >2.5 mm | GRO (pg/mL) | IL-8 (pg/mL) |
|---|---|---|---|---|---|---|---|---|---|---|
| Control | F | 32 | 426 | no | 0 | 0 | 0 | no | 2.5 | 0.3 |
| Control (N2) | F | 38 | 561 | no | 0 | 0 | 0 | no | 7.3 | 0.0 |
| Control | M | 40 | 584 | no | 0 | 0 | 0 | no | 5.9 | 1.5 |
| Control | F | 50 | 723 | no | 0 | 0 | 0 | no | 0.0 | 0.2 |
| Control | F | 53 | 486 | no | 0 | 1 | 2 | no | 2.5 | 0.1 |
| Control | F | 64 | 525 | no | 0 | 0 | 0 | no | 9.7 | 2.1 |
| Control (N1) | M | 63 | 363 | no | 0 | NA | NA | NA | 4.3 | 2.6 |
| Control (N3) | M | 25 | 299 | no | 0 | NA | NA | NA | 11.3 | 4.4 |
| *CEL* carrier | M | 9 | 448 | no | 0 | 0 | 0 | no | 2.5 | 2.0 |
| *CEL* carrier | M | 14 | 50 | no | 0 | 0 | 0 | no | 11.1 | 4.5 |
| *CEL* carrier | F | 17 | 71 | no | 0 | 1 | 6 | no | 5.1 | 5.3 |
| *CEL* carrier (P2) | M | 37 | 10 | no | 0 | 0 | 0 | no | NA | NA |
| *CEL* carrier (P1) | M | 40 | 12 | no | 0 | 0 | 0 | no | 7.3 | 7.7 |
| *CEL* carrier (D2) | F | 43 | 0 | yes | 13.1 | 12 | 7 | no | 116.7 | 21.1 |
| *CEL* carrier | F | 45 | 51 | yes | 6.2 | 9 | 4 | no | 45.1 | 16.8 |
| *CEL* carrier | M | 56 | 0 | yes | 11.8 | 6 | 4 | no | 97.3 | 4.3 |
| *CEL* carrier | M | 57 | 0 | yes | 17.5 | 4 | 11 | yes | 15.2 | 3.1 |
| *CEL* carrier (D4) | F | 57 | 5 | yes | 19.1 | 60 | 11 | no | 109.7 | 373.6 |
| *CEL* carrier (D1) | M | 65 | 0 | yes | 44.7 | 20 | 13 | no | 2.5 | 1.2 |
| *CEL* carrier (D3) | M | 69 | 3 | yes | 13.6 | 30 | 9 | no | 88.8 | 4.4 |
| *CEL* carrier (C1) | F | 78 | 0 | yes | 37.5 | 60 | 13 | no | 161.0 | 167.7 |

The alphanumeric code in the Status column is explained in RESEARCH DESIGN AND METHODS. NA, not available.

and "no enzyme") were used when MS/MS spectra were searched against the human ipi database (version 3.6) using the Sequent algorithm (version 5) (15). The data were filtered to a false discovery rate of less than 1% based on the target-decoy database approach (16). Further filtering of the list to include only "pancreas specific" proteins was based on analyses of nine different mouse tissues (17). To test the hypothesis that secretin-stimulated duodenal secretory proteins truly reflected pancreatic disease, an investigator (F.E.M.) blinded to the sample status performed unsupervised clustering analysis based on protein abundance (i.e., algorithmic classification procedure to group samples based on protein expression similarities and blinded to a knowledge of sample disease status).

### Bioinformatics Studies Using Biobase

We performed a comprehensive investigation of all proteins in the secretin-stimulated duodenal juice (not only pancreatic specific proteins) to avoid excluding proteins that are only expressed in the diseased state. We used the Biobase Explain 3.0 tool (18) to examine whether the proteins that were elevated in the secretin-stimulated duodenal juice from *CEL*-mutation carriers ($\log_2$ ratio $>1$ of protein expression) shared common upstream key nodes in pathways in physiological and pathophysiological processes (see http://www.biobase-international.com/product/explain for details).

### Other Statistical Analysis

For the analyses of cytokine levels, we used two-tailed Student *t* tests of independent groups assuming unequal variance. We used linear regression to estimate $R^2$ for the correlation of cyst number and the respective cytokines. We chose a significance level of 5% and analyzed all data using Stata 11.0 (Stata Statistical Software, Stata Corp., College Station, TX).

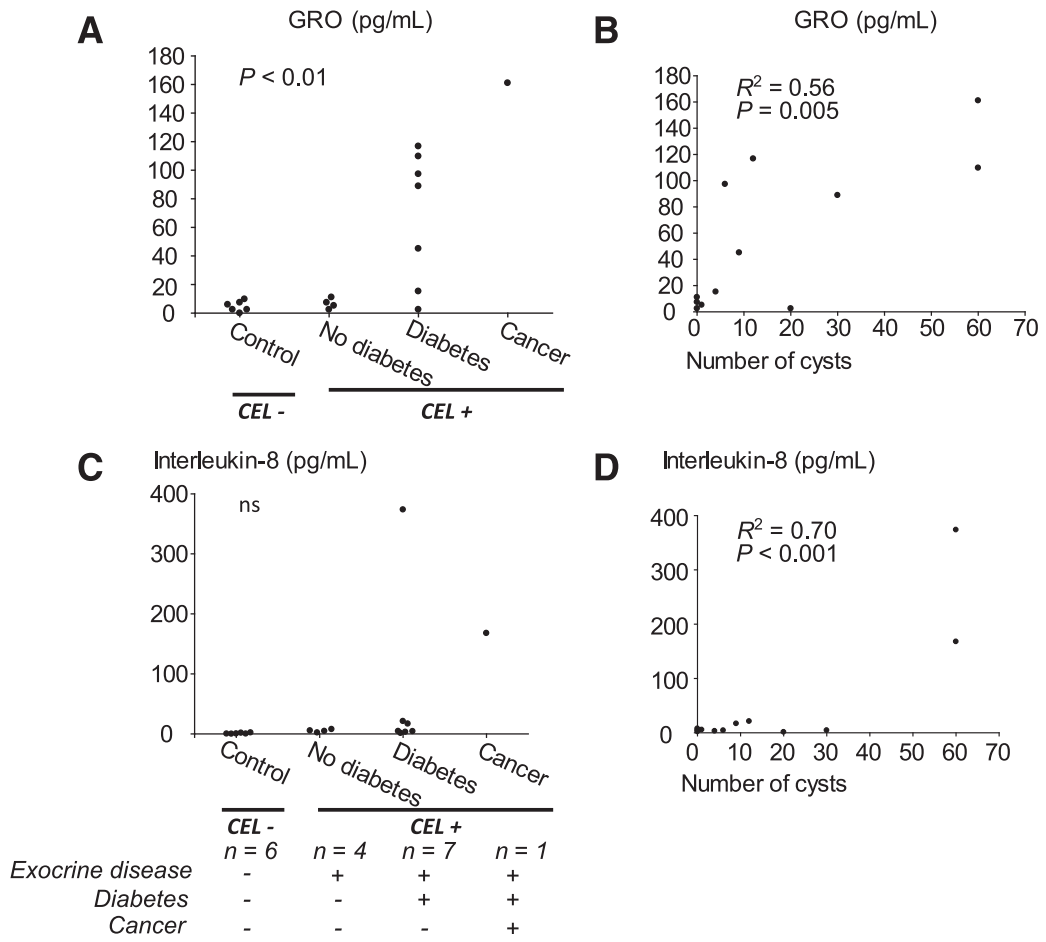


**Figure 3**—The identification of a patient-specific cytokine signature in pancreatic juice. Cytokine levels for GRO compared with mutation status (*A*) and correlated with cyst number (*B*). Cytokine levels for IL-8 compared with mutation status (*C*) and correlated with cyst number (*D*). Further, IL-1b was increased in the carriers ($P = 0.005$) and also significantly correlated with the number of cysts ($R^2 = 0.70$ $P < 0.001$). None of the remaining cytokines correlated significantly with the number of cysts but were significantly elevated in the *CEL*-mutation carriers (fibroblast growth factor-2 [$P = 0.04$], Flt-3 ligand [$P = 0.03$], granulocyte-macrophage colony–stimulating factor [$P = 0.01$], IL-1ra [$P = 0.02$], IL-12 [$P = 0.01$], MCP-1 [$P = 0.04$], soluble CD40 ligand [$P = 0.03$]; Supplementary Table 1).

## RESULTS

### Subjects With CEL-MODY Develop Multiple Pancreatic Cysts and Diabetes in Their 40s

We performed pancreatic imaging studies in a CEL-MODY family (Fig. 1) and identified multiple unilocular pancreatic cysts (Fig. 2) in all *CEL*-mutation carriers ($n$ = 8) who had also developed diabetes (Table 1). None of the nondiabetic *CEL*-mutation carriers ($n$ = 4) or the healthy controls ($n$ = 6) had multiple pancreatic cysts, but two of these subjects (one nondiabetic *CEL*-mutation carrier and one healthy control) had a solitary cyst. Moreover, the number of cysts correlated positively with age in the *CEL*-mutation carriers ($R^2$ = 0.46; $P$ = 0.01).

### Cytokine Analysis of the Secretin-Stimulated Duodenal Juice Identifies Mitogen-Activated Protein Kinase–Driven Cytokines in *CEL*-Mutation Carriers Positively Correlated With Disease Progression

Since cytokine levels in secretin-stimulated duodenal juice may reflect pancreatic disease (19), we first assessed a panel of 42 cytokines in the secretin-stimulated duodenal fluid samples of several family members and controls (Supplementary Table 1). The mitogen-activated protein kinase (MAPK)-driven CXCR2 receptor targeting cytokine GRO was significantly increased in the carriers with a tendency toward higher levels in subjects who had accumulated more clinical manifestations (Table 1 and Fig. 3*A*; $P < 0.01$). We also observed that GRO correlated significantly with the number of cysts in the subjects (Fig. 3*B*; $R^2$ = 0.56; $P$ = 0.005). Interestingly, the related MAPK-driven CXCR1- and CXCR2-targeting cytokine IL-8, while not showing significantly increased levels in *CEL*-mutation carriers (Fig. 3*C*; $P$ = 0.15), revealed a significant correlation with the number of cysts (Fig. 3*D* and Supplementary Table 1; $R^2$ = 0.72; $P < 0.001$). Hence secretin-stimulated duodenal fluid of *CEL*-mutation carriers contains cytokines whose increasing levels may potentially reflect increasing severity of a progressive pancreatic disease.

### Proteomics-Based Identification of a Distinct Protein Signature in Secretin-Stimulated Duodenal Juice of *CEL*-Mutation Carriers

Since some protein markers (cytokines) displayed increasing levels with the progressive accumulation of clinical manifestations, we asked whether diabetic

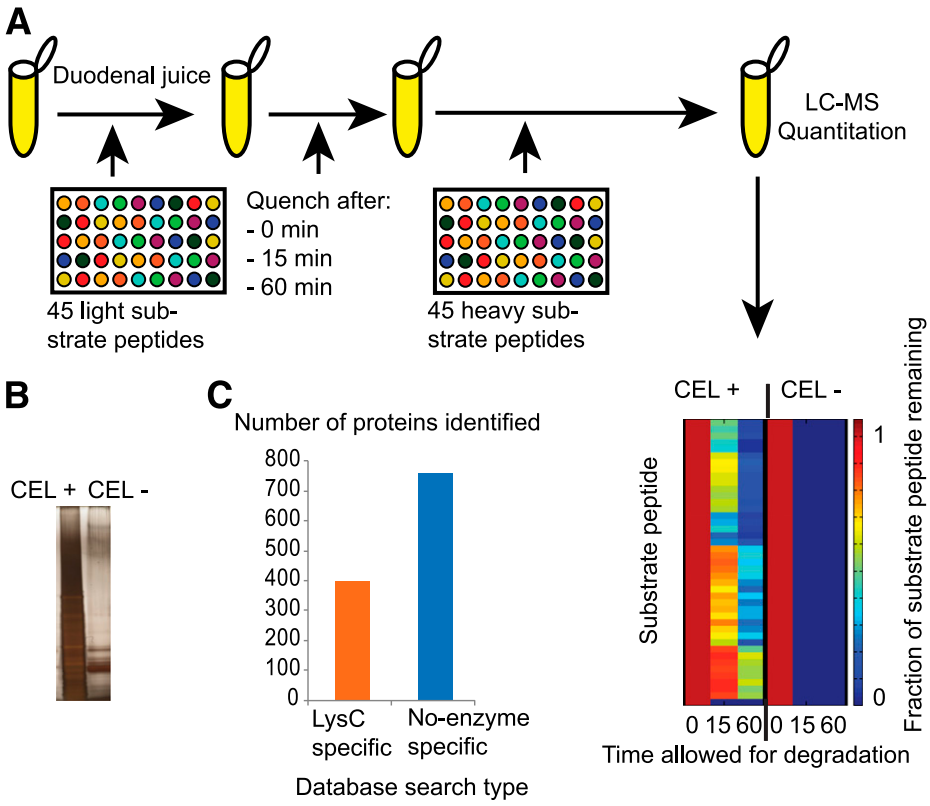


**Figure 4**—Reduced substrate degradation in CEL-MODY patients. Greater substrate degradation was observed for control patients compared with CEL-MODY patients. *A*: A set of 45 substrate peptides are incubated with pancreatic juice for 45 min, and the amount of degradation is measured by comparison of the substrate with internal standard heavy peptides at 0, 15, and 60 min time points. *B*: The differences in protein identifications using silver staining of secretin-stimulated duodenal juice for equal quantities of protein loaded onto gels. *C*: Consistent with this reduced substrate degradation in the secretin-stimulated duodenal juice of CEL-MODY patients, we also identified differences in protein identifications using LysC-and "no-enzyme"-specific searches of proteomics data. Using no-enzyme-specific searches, we identified 757 proteins in the secretin-stimulated duodenal juice.

*CEL*-mutation carriers displayed a unique proteomic signature in secretin-stimulated duodenal juice. Anticipating some degree of protein degradation in duodenal juice, we first assessed the extent of protein degradation by exploring a multiplexed MS-based degradation assay (Fig. 4*A*) and differences in silver staining for equal quantities of protein loaded onto gels (Fig. 4*B*) and found indeed an extensive degradation of secretin-stimulated duodenal proteins. Subsequently, we applied a multiplexed quantitative proteomics approach with isobaric labeling (TMT) to a training set of secretin-stimulated duodenal juice from three *CEL*-mutation carriers and three healthy controls. Consistent with the previously identified protein degradation, we found large differences in protein identifications using standard LysC compared with "no-enzyme"-specific searches of proteomics data (Fig. 4*C*). Hence, to identify both the degraded and nondegraded proteins to account for all the secreted proteins in the original sample, we further pursued no-enzyme-specified database searching, and we identified 757 proteins (1% false discovery rate) in the secretin-stimulated duodenal juice (Supplementary Table 2) despite the extensive protein degradation. Further filtering of the list to include only proteins abundantly expressed in mice pancreata (17) resulted in the identification of 115 proteins (excerpt in Table 2). Intriguingly, an unsupervised clustering analysis clearly separated the patients and the controls into two separate groups (Fig. 5*A*), supporting the existence of a unique proteomic signature (Table 2 and Supplementary Table 2) in diabetic

**Table 2—The most extreme differentially expressed proteins in secretin-stimulated duodenal juice**

| | Gene | $Log^2$ ratio | $Log^2$ total | Protein # | Gene | $Log^2$ ratio | $Log^2$ total |
|---|---|---|---|---|---|---|---|
| 1 | *CLEC3B* | −16.0 | 23.2 | 87 | *MUC1* | 2.4 | 20.2 |
| 2 | *KRT18* | −15.2 | 22.4 | 88 | *CUZD1* | 2.5 | 25.8 |
| 3 | *NUCB2* | −12.5 | 19.7 | 89 | *CLPS* | 2.6 | 22.5 |
| 4 | *DCI* | −11.5 | 19.6 | 90 | *PNLIPRP2* | 2.7 | 27.3 |
| 5 | *MYL1* | −11.5 | 18.7 | 91 | *KLK1* | 2.7 | 24.1 |
| 6 | *RPLP2* | −11.1 | 23.2 | 92 | *RNASE1* | 3.5 | 25.7 |
| 7 | *SKP1* | −10.8 | 18.1 | 93 | *CPA2* | 3.6 | 27.7 |
| 8 | *RPLP0* | −10.7 | 21.7 | 94 | *S100A7* | 3.9 | 22.4 |
| 9 | *RPLP1* | −9.7 | 21.4 | 95 | *CEL* | 3.9 | 28.5 |
| 10 | *SFN* | −9.5 | 19.1 | 96 | *CTRB1* | 3.9 | 27.8 |
| 11 | *EPB41L3* | −9.4 | 22.1 | 97 | *CTRL* | 3.9 | 23.9 |
| 12 | *CHGA* | −8.9 | 16.1 | 98 | *PRSS1* | 4.0 | 28.1 |
| 13 | *PKM2* | −7.5 | 22.3 | 99 | *CPA1* | 4.1 | 28.9 |
| 14 | *IDH1* | −7.1 | 22.5 | 100 | *CELA3B* | 4.3 | 25.6 |
| 15 | *MYH14* | −6.2 | 22.3 | 101 | *PNLIPRP1* | 4.3 | 26.3 |
| 16 | *PURA* | −6.2 | 20.7 | 102 | *IPI00219910* | 4.6 | 23.5 |
| 17 | *LMNA* | −5.5 | 21.3 | 103 | *PNLIP* | 4.8 | 30.0 |
| 18 | *KRT8* | −5.1 | 24.9 | 104 | *PRSS2* | 4.8 | 26.6 |
| 19 | *EEF1A1* | −5.1 | 21.0 | 105 | *CELA3A* | 4.9 | 27.8 |
| 20 | *GLUD1* | −4.9 | 22.5 | 106 | *CTRC* | 5.0 | 26.8 |
| 21 | *PCDH24* | −4.7 | 21.8 | 107 | *GP2* | 5.2 | 25.8 |
| 22 | *PPA1* | −4.1 | 22.1 | 108 | *CPB1* | 5.3 | 27.9 |
| 23 | *NPC2* | −4.0 | 20.2 | 109 | *AMY1C* | 5.3 | 26.8 |
| 24 | *ALDOB* | −3.8 | 25.5 | 110 | *AMY2B* | 5.4 | 29.6 |
| 25 | *TSPAN8* | −3.7 | 20.2 | 111 | *SERPINI2* | 6.7 | 22.8 |
| 26 | *CLIC1* | −3.7 | 23.0 | 112 | *PLA2G1B* | 6.9 | 25.8 |
| 27 | *PGD* | −3.7 | 19.9 | 113 | *CD302* | 8.2 | 16.7 |
| 28 | *CST3* | −3.3 | 23.5 | 114 | *HPN* | 8.4 | 18.4 |
| 29 | *GSN* | −3.3 | 24.9 | 115 | *CTRB2* | 11.3 | 18.5 |

$Log^2$ ratio, $log^2$ of the ratio of MS abundance for the sum of the three healthy controls divided by the sum of the three diabetic mutation carriers; $log^2$ total, $log^2$ of the total MS abundance for a protein as the sum of the abundances of three healthy controls and the three diabetic mutation carriers.

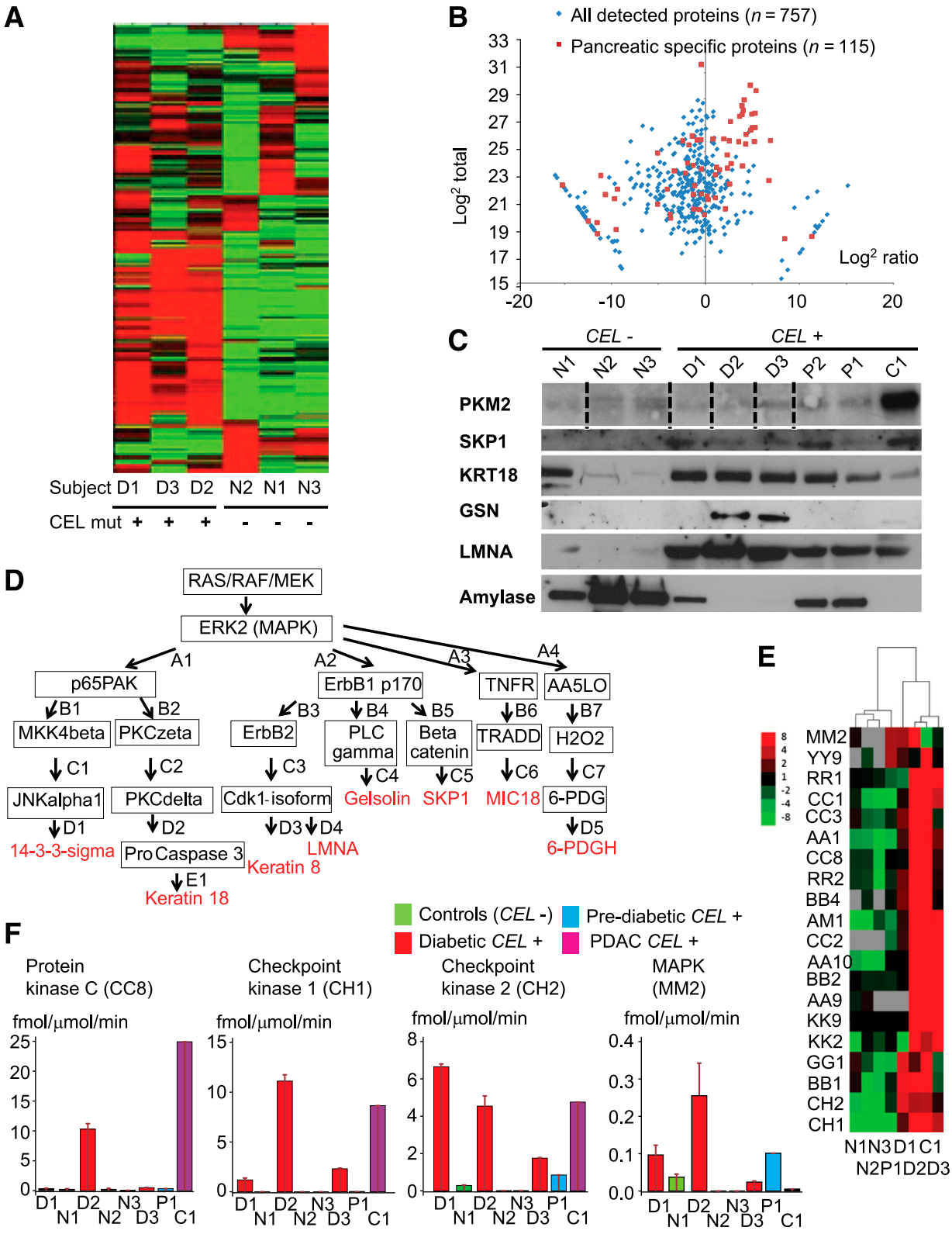


**Figure 5**—The identification of a patient-specific protein signature in pancreatic juice. Protein quantitation was performed using isobaric labeling with TMT and LC-MS/MS analysis on an LTQ-Orbitrap Velos mass spectrometer. *A*: An unsupervised clustering analysis identified clearly different expression patterns in *CEL*-mutation carriers compared with controls with analyses performed by an investigator (F.M.) blinded to the samples. *B*: $Log^2$ plot of secretin-stimulated duodenal protein abundances and ratios of levels in the three *CEL*-mutation carriers compared with the three controls. Note the lack of skewed distribution of pancreatic proteins in the $log^2$ plot, indicating that a majority of the proteins had been detected despite degradation. Using "no-enzyme"-specific searches, we identified 757 proteins in the secretin-stimulated duodenal juice, of which 115 proteins were pancreatic specific based on a previous report (17). *C*: Immunoblot validation examples of proteins identified with stippled lines indicate gel crops. In addition to the three diabetic *CEL*-mutation carriers (D1,

*CEL*-mutation carriers. We identified mostly digestive enzymes (Table 2) among the duodenal proteins showing a relatively higher abundance in control samples (Fig. 5*B*), including CEL and elastase (CELA2A, CELA3B), consistent with our anticipation of a greater abundance of pancreatic proteases in healthy subjects. Proteins more abundant in *CEL*-mutation carriers (Table 2) included proteins associated with diabetes [TSPAN8 (20)] and insulin secretion [GLUD1 (21)]. Together these observations provide confidence that secretin-stimulated duodenal proteins actually reflect pancreatic output and could serve as potential indicators of pancreatic pathology.

### Validation of the Training Set Proteins by Immunoblotting and Their Potential Role as MAPK Targets

Next, to validate the proteome signature in *CEL*-mutation carriers, we applied immunoblotting of selected signature proteins in secretin-stimulated duodenal juice from the training set of three *CEL*-mutation carriers and three controls. Indeed, band intensities and MS abundances correlated well for the proteins (compare Fig. 5*C* and Supplementary Table 2), confirming the validity of the MS findings. Furthermore, band intensities were also clearly different between controls and two additional prediabetic *CEL*-mutation carriers (Fig. 5*C*). Notably, the protein markers LMNA, SKP1, and Keratin 18 (*KRT18*) clearly separated *CEL*-mutation carriers from controls, whereas the protein markers PKM2 and GSN more partially separated these groups. In order to assess whether the proteome signature proteins in *CEL*-mutation carriers were parts of an activated pathway, we explored the potential connectivity of the top 30 most abundant proteins in the training set using a curated database search (Biobase Explain) of reported protein interactions (18). Intriguingly, we found that several of these validated markers were downstream targets of MAPK (Fig. 5*D* and Supplementary Table 3), including several of the proteins also validated by immunoblotting (compare Fig. 5*D* with Fig. 5*C*).

To further assess the strength of connectivity between the most abundant proteins, we used gene network enrichment analysis (22,23) to test for significant protein interactions based on yeast two-hybrid systems data. We identified the 14–3-3 protein ζ, encoded by *YWHAZ,* interacting with *KRT18* and the subnetwork of interacting proteins around *YWHAZ* to be cumulatively significant (Fisher's $P = 0.00028$), supporting interactions between 14–3-3 protein ζ and *KRT18* in disease pathogenesis (Supplementary Fig. 1). Both these proteins were also MAPK targets as defined by the Biobase Explain findings.

### Multiplexed Kinase Studies Provide Further Evidence of Altered Kinase Activity

Since the above data suggested the involvement of MAPK signaling, we profiled multiple kinase activities in both duodenal samples using MS (Fig. 5*E*) (14). Upon examining a different aliquot of the same secretin-stimulated duodenal juice samples as that used in the immunoblotting studies and adopting unsupervised clustering analysis, we observed that the three controls and the prediabetic *CEL*-mutation carrier clustered in one group clearly different from a group with the four diabetic *CEL*-mutation carriers (including a subject with pancreatic ductal adenocarcinoma). Interestingly, the cell-cycle-related kinases, CHK1 and CHK2, and protein kinase C (PKC) and to a lesser extent also MAPK displayed elevated kinase activity in the diabetic *CEL*-mutation carriers (Fig. 5*F*).

## DISCUSSION

Our data further support that CEL-MODY is a progressive disease. We have previously reported the occurrence of pancreatic exocrine dysfunction from infancy (3), pancreatic lipomatosis form early childhood (4), and diabetes developing in the 40s (3). Here we show that CEL-mutation carriers also develop multiple pancreatic cysts as they develop diabetes. Thus there seems to be a sequence of clinical characteristics over time that may reflect a pathogenic process taking place in the pancreas and ultimately leading to diabetes. Our data support that this pathogenic process is associated with upregulated MAPK signaling for the following reasons: First, cytokine analyses in the pancreatic secretome demonstrated increasing levels of the MAPK-driven (24) cytokine GRO over the course of the disease. Second, using a sensitive and accurate quantitative proteomics approach, we identified elevated levels of downstream target proteins

D2, D3) and three nonfamily controls (N1, N2, N3), we also added secretin-stimulated duodenal juice samples from two prediabetic *CEL*-mutation carriers (P1, P2) and from the *CEL*-mutation carrier with the *KRAS*-mutated pancreatic ductal adenocarcinoma (C1). *D*: Visualization of the MAPK-targeted proteins identified by Biobase ExPlain 3.0 tool and alphanumeric codes referring to PubMed identification in Supplementary Table 3. *E*: Heat map demonstrating differential clustering of kinase activities in the secretin-stimulated duodenal juice and pancreatic tissue of *CEL*-mutation carriers and controls. *F*: Vertical bar graphs showing significant differences in kinase activities for PKC, CH1, and CH2 in secretin-stimulated duodenal juice. The multiplexed kinase activity assay allows the absolute quantitation of kinase activities by measuring the amount of phosphorylation of 60 peptide substrates with known motifs for many kinases. Vertical bar graphs showing differences in kinase activities for PKC, CH1, CH2, and MAPK in secretin-stimulated duodenal juice. PDAC, pancreatic ductal adenocarcinoma; mut, mutation; $\log^2$ ratio, $\log^2$ of the ratio of MS abundance for the sum of the three controls divided by the sum of the three diabetic mutation carriers; $\log^2$ total, $\log^2$ of the total MS abundance for a protein as the sum of the abundances of three controls and the three diabetic mutation carriers.

of MAPK/ERK2 signaling in diabetic *CEL*-mutation carriers. Third, the MS data were confirmed by immunoblotting for proteins in the duodenal juice, and immunoblotting also confirmed our observations in several other *CEL*-mutation-carrying subjects. Finally, we identified elevated kinase activity, including that of MAPK in *CEL*-mutation carriers.

Our data also support our hypothesis that secretin-stimulated duodenal secretory proteins truly reflect pancreatic disease. First, unsupervised clustering analysis of proteomics data correctly identified the diseased subjects. Second, we also detected increased levels of digestive enzymes in healthy subjects consistent with our anticipation of a greater abundance of pancreatic proteases in healthy subjects and consistent with proteomics findings in normal pancreatic juice by endoscopic retrograde cholangiopancreatography (25), by enzymatic findings (of elastase) in feces (3), and by enzymatic findings (of amylase, lipase, and chymotrypsin) in the secretin-stimulated duodenal juice of *CEL*-mutation carriers (26). Third, the increased levels of digestive enzymes were confirmed by immunoblotting (for amylase).

We have described a new feature of the CEL-MODY phenotype by demonstrating the presence of pancreatic cysts in mutation carriers. Such cysts are an established risk factor for pancreatic cancer (27). Notably, one of the oldest affected members of the family was diagnosed with pancreatic ductal adenocarcinoma at 78 years of age. We therefore conclude that CEL-MODY patients could be at increased risk for developing pancreatic cancer. The cytokine analyses revealed a linear relationship between the number of cysts and the CXCR1-and CXCR2-targeting MAPK-driven (24) cytokines (GRO, IL-8), a finding consistent with a previous report of elevated IL-8 levels in sera of patients with pancreatic cancer (28). We believe that the low levels of GRO and IL-8, despite multiple cysts in a diabetic *CEL*-mutation carrier (subject D1), fit with the long duration of his diabetes and the development of end-stage pancreatic disease with loss of inflammatory cells as observed in end-stage pancreatitis (29), although there is also the possibility of phenotypic variance within the family. The finding of MAPK-related proteins and cytokines in duodenal juice of subjects with progressive pancreatic disease is particularly interesting because of the role of MAPK both in diabetes and cancer (30). In the subject with cancer, the tumor had a somatic *KRAS* mutation (G12V, not shown) commonly observed in pancreatic adenocarcinomas (31). Cancer-associated *KRAS* mutations generally lead to overactive proteins that stimulate oncogenic signaling through the MAPK pathway (32).

In conclusion, subjects with CEL-MODY develop multiple pancreatic cysts and diabetes in their 40s. Increased levels of MAPK target proteins may reflect the pathophysiological development of pancreatic cysts and diabetes in CEL-MODY. These data suggest that the MAPK pathway should be further explored in subjects with CEL-MODY in order to find drug targets for the possible prevention of disease development.

**Acknowledgments.** The authors thank C.R. Kahn and C.W. Liew of Joslin Diabetes Center for discussions, G. Sankaranarayanan of Joslin Diabetes Center for assistance with cytokine assays, C. Cahill of Joslin Diabetes Center for assistance with electron microscopy, and E. Huttlin of Harvard Medical School for assistance with data analysis of pancreatic-specific proteins.

**Funding.** This work was supported by the Norwegian Research Council (to H.R. and P.R.N.); the Western Norway Regional Health Authority (to H.R., H.I., and P.R.N.); the Norwegian Endocrine Society and the Fulbright Foundation (to H.R.); Innovest and the University of Bergen (to P.R.N.); the Norwegian Cancer Society (to A.M.); Joslin DRC Specialized Assay and Advanced Microscopy Cores (NIH P30 DK-36836), National Institutes of Health grant HG3456 (to S.P.G.), and National Institutes of Health grant RO1 DK-67536 and the Graetz Bridge Funds (to R.N.K.).

**Duality of Interest.** No potential conflicts of interest relevant to this article were reported.

**Author Contributions.** H.R. and R.N.K. designed the study, contributed to data analysis and interpretation, and drafted the manuscript with input from all others. F.E.M., E.T., S.B., and I.H. collected data and contributed to data analysis and interpretation. J.H., S.M.W., M.V., A.E.O., D.H., and G.D. collected data. M.L., M.B.R., H.I., P.R.N., and A.M. contributed to data analysis and interpretation. S.P.G. designed the study and contributed to data analysis and interpretation. H.R. and R.N.K. are the guarantors of this work and, as such, had full access to all data in the study and take responsibility for the integrity of the data and accuracy of the data analysis.

## References

1. Pearson ER, Starkey BJ, Powell RJ, Gribble FM, Clark PM, Hattersley AT. Genetic cause of hyperglycaemia and response to treatment in diabetes. Lancet 2003;362:1275–1281
2. Ashcroft FM, Rorsman P. Diabetes mellitus and the β cell: the last ten years. Cell 2012;148:1160–1171
3. Raeder H, Johansson S, Holm PI, et al. Mutations in the CEL VNTR cause a syndrome of diabetes and pancreatic exocrine dysfunction. Nat Genet 2006;38:54–62
4. Raeder H, Haldorsen IS, Ersland L, et al. Pancreatic lipomatosis is a structural marker in nondiabetic children with mutations in carboxyl-ester lipase. Diabetes 2007;56:444–449
5. Lombardo D. Bile salt-dependent lipase: its pathophysiological implications. Biochim Biophys Acta 2001;1533:1–28
6. Vesterhus M, Raeder H, Kurpad AJ, et al. Pancreatic function in carboxyl-ester lipase knockout mice. Pancreatology 2010;10:467–476
7. Ræder H, Vesterhus M, El Ouaamari A, et al. Absence of diabetes and pancreatic exocrine dysfunction in a transgenic model of carboxyl-ester lipase-MODY (maturity-onset diabetes of the young). PLoS ONE 2013;8:e60229
8. Johansson BB, Torsvik J, Bjørkhaug L, et al. Diabetes and pancreatic exocrine dysfunction due to mutations in the carboxyl ester lipase gene-maturity onset diabetes of the young (CEL-MODY): a protein misfolding disease. J Biol Chem 2011;286:34593–34605
9. Paulo JA, Lee LS, Wu B, Banks PA, Steen H, Conwell DL. Mass spectrometry-based proteomics of endoscopically collected pancreatic fluid in chronic pancreatitis research. Proteomics Clin Appl 2011;5:109–120
10. Ting L, Rad R, Gygi SP, Haas W. MS3 eliminates ratio distortion in isobaric multiplexed quantitative proteomics. Nat Methods 2011;8:937–940
11. Kunz RC, McAllister FE, Rush J, Gygi SP. A high-throughput, multiplexed kinase assay using a benchtop orbitrap mass spectrometer to investigate

the effect of kinase inhibitors on kinase signaling pathways. Anal Chem 2012;84:6233–6239

12. Stevens T, Conwell DL, Zuccaro G Jr, Lewis SA, Love TE. The efficiency of endoscopic pancreatic function testing is optimized using duodenal aspirates at 30 and 45 minutes after intravenous secretin. Am J Gastroenterol 2007;102:297–301
13. Stevens T, Conwell DL, Zuccaro G Jr, Vargo JJ, Dumot JA, Lopez R. Comparison of endoscopic ultrasound and endoscopic retrograde pancreatography for the prediction of pancreatic exocrine insufficiency. Dig Dis Sci 2008;53:1146–1151
14. Kubota K, Anjum R, Yu Y, et al. Sensitive multiplexed analysis of kinase activities and activity-based kinase identification. Nat Biotechnol 2009;27:933–940
15. Eng JK, McCormack AL, Yates JR 3rd. An approach to correlate tandem mass spectral data of peptides with amino acid sequences in a protein database. J Am Soc Mass Spectrom 1994;5:976–989
16. Elias JE, Gygi SP. Target-decoy search strategy for increased confidence in large-scale protein identifications by mass spectrometry. Nat Methods 2007;4:207–214
17. Huttlin EL, Jedrychowski MP, Elias JE, et al. A tissue-specific atlas of mouse protein phosphorylation and expression. Cell 2010;143:1174–1189
18. Kel A, Voss N, Valeev T, Stegmaier P, Kel-Margoulis O, Wingender E. ExPlain: finding upstream drug targets in disease gene regulatory networks. SAR QSAR Environ Res 2008;19:481–494
19. Paulo JA, Lee LS, Wu B, Banks PA, Steen H, Conwell DL. Cytokine profiling of pancreatic fluid using the ePFT collection method in tandem with a multiplexed microarray assay. J Immunol Methods 2011;369:98–107
20. Craddock N, Hurles ME, Cardin N, et al.; Wellcome Trust Case Control Consortium. Genome-wide association study of CNVs in 16,000 cases of eight common diseases and 3,000 shared controls. Nature 2010;464:713–720
21. Stanley CA, Lieu YK, Hsu BY, et al. Hyperinsulinism and hyperammonemia in infants with regulatory mutations of the glutamate dehydrogenase gene. N Engl J Med 1998;338:1352–1357
22. Liu M, Liberzon A, Kong SW, et al. Network-based analysis of affected biological processes in type 2 diabetes models. PLoS Genet 2007;3:e96
23. Mori MA, Liu M, Bezy O, et al. A systems biology approach identifies inflammatory abnormalities between mouse strains prior to development of metabolic disease. Diabetes 2010;59:2960–2971
24. Ancrile BB, O'Hayer KM, Counter CM. Oncogenic ras-induced expression of cytokines: a new target of anti-cancer therapeutics. Mol Interv 2008;8:22–27
25. Zhou L, Lu Z, Yang A, et al. Comparative proteomic analysis of human pancreatic juice: methodological study. Proteomics 2007;7:1345–1355
26. Tjora E, Wathle G, Engjom T, et al. Severe Pancreatic Dysfunction But Compensated Nutritional Status in Monogenic Pancreatic Disease Caused by Carboxyl-Ester Lipase Mutations. Pancreas 2013;42:1078–1084
27. Tanaka S, Nakao M, Ioka T, et al. Slight dilatation of the main pancreatic duct and presence of pancreatic cysts as predictive signs of pancreatic cancer: a prospective study. Radiology 2010;254:965–972
28. Wigmore SJ, Fearon KC, Sangster K, Maingay JP, Garden OJ, Ross JA. Cytokine regulation of constitutive production of interleukin-8 and -6 by human pancreatic cancer cell lines and serum cytokine concentrations in patients with pancreatic cancer. Int J Oncol 2002;21:881–886
29. Braganza JM, Lee SH, McCloy RF, McMahon MJ. Chronic pancreatitis. Lancet 2011;377:1184–1197
30. Lawrence MC, Jivan A, Shao C, et al. The roles of MAPKs in disease. Cell Res 2008;18:436–442
31. Immervoll H, Hoem D, Kugarajh K, Steine SJ, Molven A. Molecular analysis of the EGFR-RAS-RAF pathway in pancreatic ductal adenocarcinomas: lack of mutations in the BRAF and EGFR genes. Virchows Arch 2006;448:788–796
32. Collisson EA, Trejo CL, Silva JM, et al. A central role for RAF→MEK→ERK signaling in the genesis of pancreatic ductal adenocarcinoma. Cancer Discov 2012;2:685–693